

## Highlights

### **A Robust Real-Time Lane Detection Method with Fog-Enhanced Feature Fusion for Foggy Conditions**

Ronghui Zhang, Yuhang Ma, Tengfei Li, Ziyu Lin, Yueying Wu, Junzhou Chen, Lin Zhang, Jia Hu, Tony Z. Qiu, Konghui Guo

arXiv:2504.06121v10 [cs.CV] 20 Oct 2025

- A new real-world dataset and two synthetic datasets for foggy lane detection are proposed.
- A novel Fog-Enhanced Network is proposed for lane detection in fog.
- Three core modules are designed to enhance feature extraction in fog.
- The method achieves SOTA performance with real-time speed on embedded devices.

# A Robust Real-Time Lane Detection Method with Fog-Enhanced Feature Fusion for Foggy Conditions

Ronghui Zhang<sup>a</sup>, Yuhang Ma<sup>a</sup>, Tengfei Li<sup>a</sup>, Ziyu Lin<sup>a</sup>, Yueying Wu<sup>a</sup>, Junzhou Chen<sup>a,\*</sup>, Lin Zhang<sup>b</sup>, Jia Hu<sup>c</sup>, Tony Z. Qiu<sup>d</sup>,  
Konghui Guo<sup>e</sup>

<sup>a</sup>Guangdong Key Laboratory of Intelligent Transportation System, School of Intelligent Systems Engineering, Sun Yat-sen University, Guangzhou, 510275, China

<sup>b</sup>College of Automotive Studies, Tongji University, Shanghai, 201804, China

<sup>c</sup>College of Transportation Engineering, Tongji University, Shanghai, 201804, China

<sup>d</sup>Department of Civil and Environmental Engineering, University of Alberta, Edmonton, Alberta, Canada

<sup>e</sup>State Key Laboratory of Automotive Chassis Integration and Bionics, Jilin University, Changchun, 130025, China

---

## Abstract

Lane detection is a critical component of Advanced Driver Assistance Systems (ADAS). Existing lane detection algorithms generally perform well under favorable weather conditions. However, their performance degrades significantly in adverse conditions, such as fog, which increases the risk of traffic accidents. This challenge is compounded by the lack of specialized datasets and methods designed for foggy environments. To address this, we introduce the FoggyLane dataset, a diverse and comprehensive benchmark captured in real-world foggy scenarios across multiple road types and conditions, and synthesize two more datasets, FoggyCULane and FoggyTusimple, derived from widely used lane detection datasets. Furthermore, we propose a robust Fog-Enhanced Network for lane detection, incorporating a Global Feature Fusion Module (GFFM) to capture global relationships in foggy images, a Kernel Feature Fusion Module (KFFM) to model the structural and positional relationships of lane instances, and a Low-level Edge Enhanced Module (LEEM) to address missing edge details in foggy conditions. Comprehensive experiments demonstrate that our method achieves state-of-the-art performance, with F1-scores of 95.04 on FoggyLane, 79.85 on FoggyCULane, and 96.95 on FoggyTusimple. Additionally, with TensorRT acceleration, the method reaches a processing speed of 38.4 FPS on the NVIDIA Jetson AGX Orin, confirming its real-time capabilities and robustness in foggy environments.

*Keywords:* ADAS, Intelligent vehicle, Foggy lane detection dataset, Foggy lane detection, Global attention, Edge enhancement

---

## 1. Introduction

Lane detection plays an important role in Advanced Driver Assistance Systems (ADAS), providing essential support for lane keeping, autonomous navigation, and lane departure warnings, which help reduce the risk of lane-deviation accidents[1]. As intelligent driving technologies advance, the need for robust and real-time lane detection in complex road environments is becoming more apparent, making it a key research focus in autonomous driving[2].

Under good weather and clear lane markings, current lane detection algorithms perform well. However, in complex road environments and poor weather, such as those with poor weather conditions like fog, lane markings can become blurred, image quality may decrease, and global environmental information is often obscured, which makes lane detection more challenging.

In these conditions, existing algorithms often struggle and may fail, leading to an increased risk of traffic accidents with more severe consequences. Ensuring safe driving in these conditions calls for the development of high-precision, highly robust lane detection methods optimized for foggy environments. As shown in Fig. 1, the in-vehicle camera captures real-time road images, which are preprocessed by edge devices and then sent to the lane detection module. Detected lane information is fused with data from other sensors, such as radar and GPS, along with real-time traffic data from the cloud. This information is processed in the vehicle's computing unit, allowing the system to make adaptive driving decisions—such as accelerating, braking, or steering—to ensure safety in challenging environments like fog.

Earlier lane detection algorithms [4, 5] primarily relied on traditional computer vision methods, such as feature-based approaches that detect vanishing points, use color features, and apply edge detection or line detection techniques like Hough transforms. These methods are efficient for real-time applications but require manual parameter tuning and often struggle in challenging scenarios like worn or occluded lane markings.

With the rise of deep learning, many modern lane detection methods [6, 7, 8, 9, 10, 11] leverage CNNs, which automatically extract features from raw data and generalize bet-

---

\*Corresponding author

Email addresses: zhangrh25@mail.sysu.edu.cn (Ronghui Zhang),  
mayh39@mail2.sysu.edu.cn (Yuhang Ma),  
litf23@mail2.sysu.edu.cn (Tengfei Li),  
linzy88@mail2.sysu.edu.cn (Ziyu Lin), wuyy236@mail2.sysu.edu.cn  
(Yueying Wu), chenjunzhou@mail.sysu.edu.cn (Junzhou Chen),  
tongjizl@tongji.edu.cn (Lin Zhang), hujia@tongji.edu.cn (Jia Hu),  
zhijunqiu@ualberta.ca (Tony Z. Qiu), guokh@jlu.edu.cn (Konghui Guo)

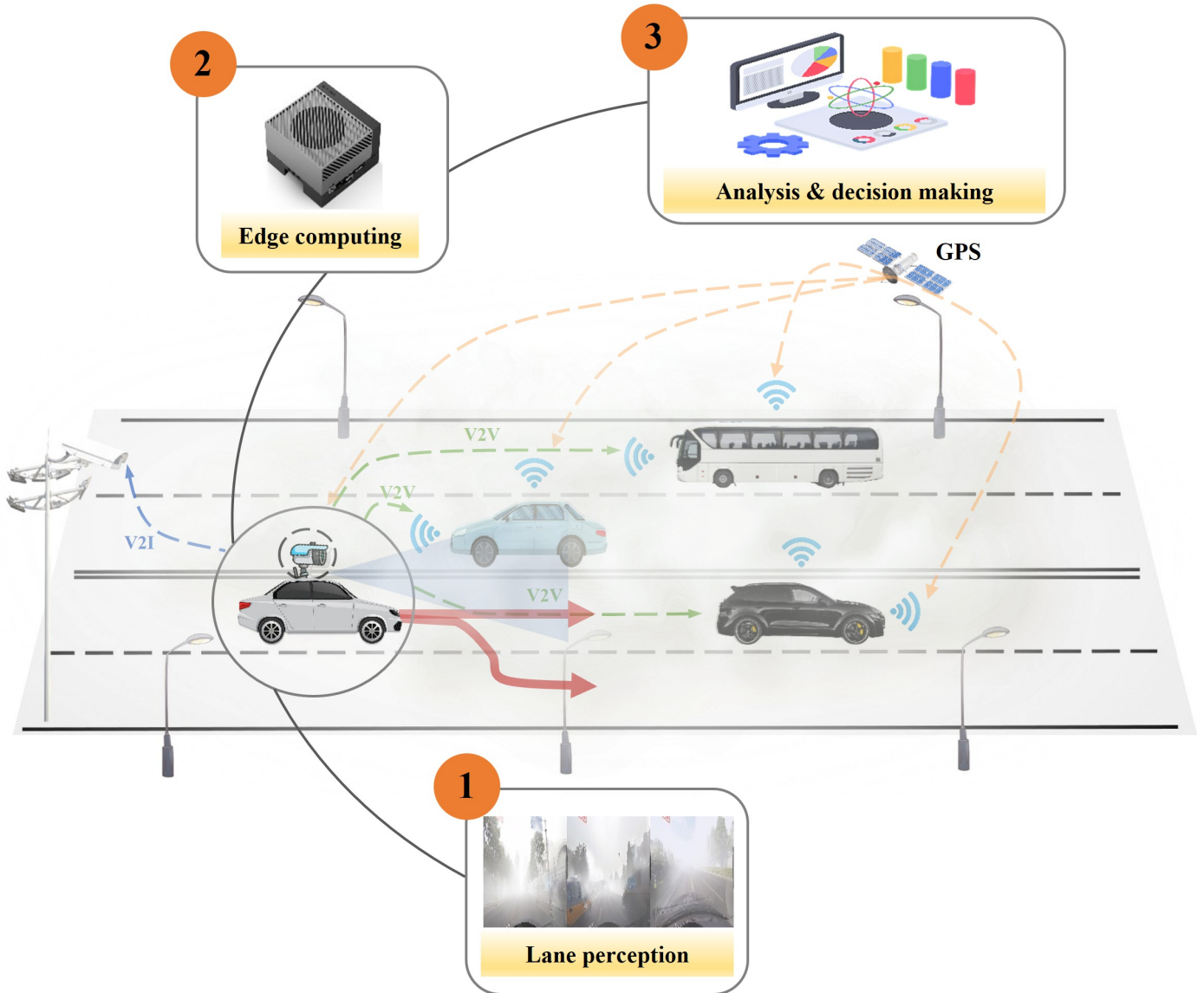


Figure 1: Lane detection in foggy scenarios for ADAS.[3]

ter in complex road environments. While deep learning provides higher robustness, many models still rely on pixel-by-pixel classification, which is computationally expensive and unnecessary for lane detection. Moreover, lane detection doesn't always require dense pixel segmentation, which can be inefficient.

Additionally, some approaches have incorporated anchor-based methods from object detection to improve efficiency and accuracy, particularly for complex or occluded lanes. These methods preset anchors at different starting points and slopes to optimize lane shape and position prediction [12, 13, 14, 15, 16]. However, these techniques still face challenges in handling foggy conditions, where image degradation severely impacts lane visibility. Traditional image enhancement methods, like dehazing, are commonly used to improve clarity but do not always result in better detection performance [17]. Some approaches generate synthetic foggy images for data augmenta-

tion, but these do not always capture real-world complexities [18].

Moreover, domain adaptation techniques [19, 20, 21, 22, 23] have been employed to bridge the gap between foggy and clear-weather images. These methods often rely on labeled clear-weather datasets or use transfer learning, but they do not fully address the unique challenges posed by foggy conditions.

Lane detection enables key functionalities such as lane departure warnings and autonomous navigation in ADAS. While existing lane detection algorithms perform well under clear weather conditions with visible lane markings, their performance drops significantly in adverse environments like fog, where reduced visibility and image degradation obscure lane clarity, thus increasing the risk of traffic accidents. Furthermore, the lack of specialized datasets tailored to foggy conditions has limited the development of effective deep learning-based solutions for these challenging scenarios.

To address these limitations, we introduce the FoggyLane dataset, a new benchmark specifically designed for lane detection under foggy conditions. This dataset, comprising 1,423 annotated images across six distinct foggy road scenarios, fills a crucial gap in the current lane detection datasets. Additionally, we create foggy versions of two commonly used lane detection datasets, CULane [8] and Tusimple [24], resulting in the FoggyCULane and FoggyTusimple datasets. These datasets are essential for training and testing lane detection algorithms in foggy environments.

In response to the unique challenges posed by foggy conditions, we propose a robust real-time lane detection method optimized for such environments. The main contributions of our work are as follows:

- 1) To address the issue of missing global information in foggy images, we design a Global Feature Fusion Module (GFFM) within the backbone network to capture relationships between inputs, improving feature extraction in foggy scenarios.
- 2) To enhance the utilization of structural relationships between lane instances, we introduce a Kernel Feature Fusion Module (KFFM) that learns and predicts the correlations between lane instances, improving lane detection accuracy and robustness.
- 3) To tackle the loss of edge information in foggy images, we incorporate a Low-level Edge Enhancement Module (LEEM), which improves the model’s sensitivity to fine edge details, ensuring better lane delineation even when visibility is severely impaired by fog.
- 4) To address the lack of open-source foggy lane detection datasets, we construct FoggyLane, a real-world dataset with 1,423 annotated images, and generate FoggyCULane and FoggyTusimple based on existing datasets. Our method achieves state-of-the-art performance with inference speeds of 192.9 FPS on NVIDIA RTX 3090 and 38.4 FPS on NVIDIA Jetson AGX Orin, confirming its real-time capability and practical applicability in real-world settings.

## 2. Related Work

In recent years, advances in deep learning have substantially improved lane detection performance. Building on these advances, current lane detection methods are divided into four main paradigms: segmentation-based, anchor-based, curve-based, and row-wise-based approaches, according to their modeling strategies.

### 2.1. Segmentation-based Lane Detection

Segmentation-based methods mainly utilize semantic segmentation or instance segmentation techniques to distinguish lane lines from other objects or backgrounds in the image, transforming lane detection into a pixel-level classification problem. LaneNet[6] employs a two-branch structure of split

branches and embedded branches, the split branches output a binary lane mask to recognize lane lines, and the embedded branches assign a unique embedding to each pixel to realize the distinction of lane lines. SCNN[8] modifies the conventional layer-wise convolution approach by incorporating a slice-wise convolution technique, enabling horizontal and vertical information flow between pixels within a layer. RESA[25] introduces a spatial attention module that ensures robust lane prediction by cyclically shifting the feature map horizontally and vertically so that each pixel can acquire global information. Although these segmentation-based methods possess high accuracy and robustness, the models are bulky and slow to process due to high consumption of computational resources. HW-Transformer[26] presents an innovative lane detection network to expand the visual range around the lane and enable global information communication through intersecting features, alongside a self-attention knowledge distillation (SAKD) method to enhance performance and semantic feature learning.

### 2.2. Curve-based Lane Detection

Curve-based methods transform the lane detection into a regression task by predicting polynomial coefficients that fit lane lines to polynomial equations. PolyLaneNet[27] proposes an end-to-end convolutional neural network that transforms images into polynomials representing each lane’s markers, along with domain-specific lane polynomials and confidence values for every lane. Similarly, LSTR[28] utilizes a Transformer-based architecture that captures both local lane structures and broader contextual information through non-local interactions. DBNet[29] introduces NURBS curves and utilizes their geometric semantic properties to achieve local and global optimization, which improves the robustness of lane line detection and model interpretation. However, polynomial fitting is sensitive to parameter selection, and minor changes in parameters can result in significant variations in fitting results, leading to unstable lane line detection.

### 2.3. Anchor-based Lane Detection

Anchor-based approaches employ predetermined reference lines within the image space to generate lane predictions, subsequently calculating necessary offsets to precisely match these anchors with true lane markings. Line-CNN[30] introduces the anchor mechanism into lane detection for the first time, and innovatively proposes line anchors. LaneATT[31] effectively solves the problem of occlusion and illumination due to the lack of a line anchor, by fusing extracted anchor features with global features generated by attention module. CLRNet[16] employs a coarse-to-fine detection strategy, where lane lines are first approximated using high-level semantic cues before being refined with detailed low-level features. This hierarchical fusion of semantic information significantly improves detection precision. FLAMNet[32] employs an adaptive line anchor strategy, augmented by patch-based feature pooling and decomposed self-attention mechanisms. This design strengthens both local feature extraction and global context modeling, improving performance in handling intricate lane structures. However, due to the

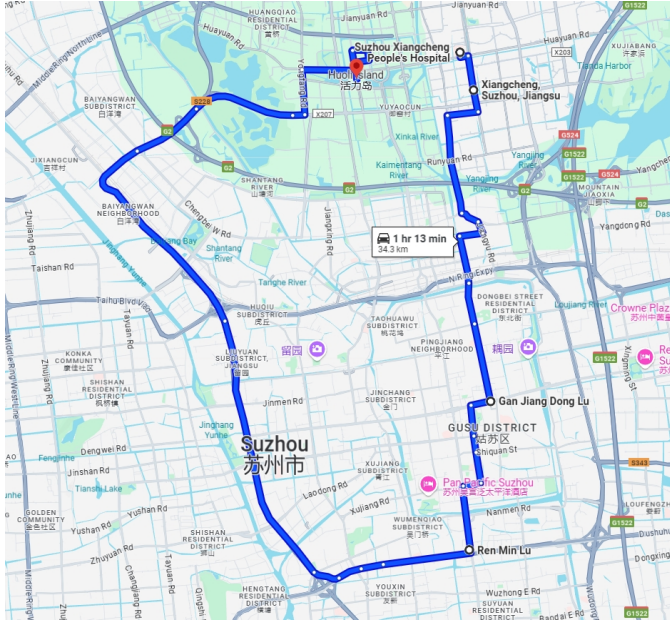


Figure 2: The route for dataset acquisition in Suzhou on the morning of October 26, 2023.[33]

multiple curvature and orientation variations of lane lines in the real world, the performance of the anchor-based methods may be limited in capturing precise paths with complex shapes.

#### 2.4. Row-wise-based Lane Detection

Row-wise methods predict lane positions for each image row. E2E-LMD[34] introduces the row-wise-based lane detection task and develops a complete architecture that outputs lane marker positions directly. UFLD[35] utilizes global features to select the lane positions of predefined rows of an image and proposes a structural loss function, so as to ensure the

continuity and smoothness of the lanes. CondLaneNet[36] utilizes conditional convolution and row-by-row prediction strategies to enhance lane recognition accuracy, and introduces the RIM module to effectively address complex lane layouts. The row-wise-based detection methods improve computational efficiency by focusing only on the row regions in the image, and possesses high detection accuracy while maintaining efficiency.

### 3. Data Construction

Due to the data-driven nature of deep learning models, the quality, size, and diversity of the datasets largely determine the applicability and performance of such models. In the task of lane detection, models trained solely on clear weather data struggle to adapt to low-visibility foggy conditions. Issues such as blurred lane boundaries, faded lane colors, and reduced image quality often arise in fog, making lane detection more challenging. Therefore, training with a foggy weather lane dataset can significantly improve an autonomous driving system’s ability to handle such conditions, enhancing both detection accuracy and overall reliability. However, there is currently no publicly available foggy weather lane detection dataset. To fill this gap, we created the FoggyLane dataset for lane detection in foggy weather. In addition, we generated two supplementary datasets, FoggyCULane and FoggyTusimple, by using fog modeling techniques on existing CULane [8] and Tusimple [24] datasets to test the generalizability of our methods.

#### 3.1. FoggyLane

Existing lane detection algorithms for intelligent connected vehicle ADAS systems perform well under favorable weather conditions, but their performance significantly deteriorates in adverse conditions like fog, which reduces visibility and increases the likelihood of traffic accidents. Current benchmark datasets, including CULane[8], Tusimple[24], and

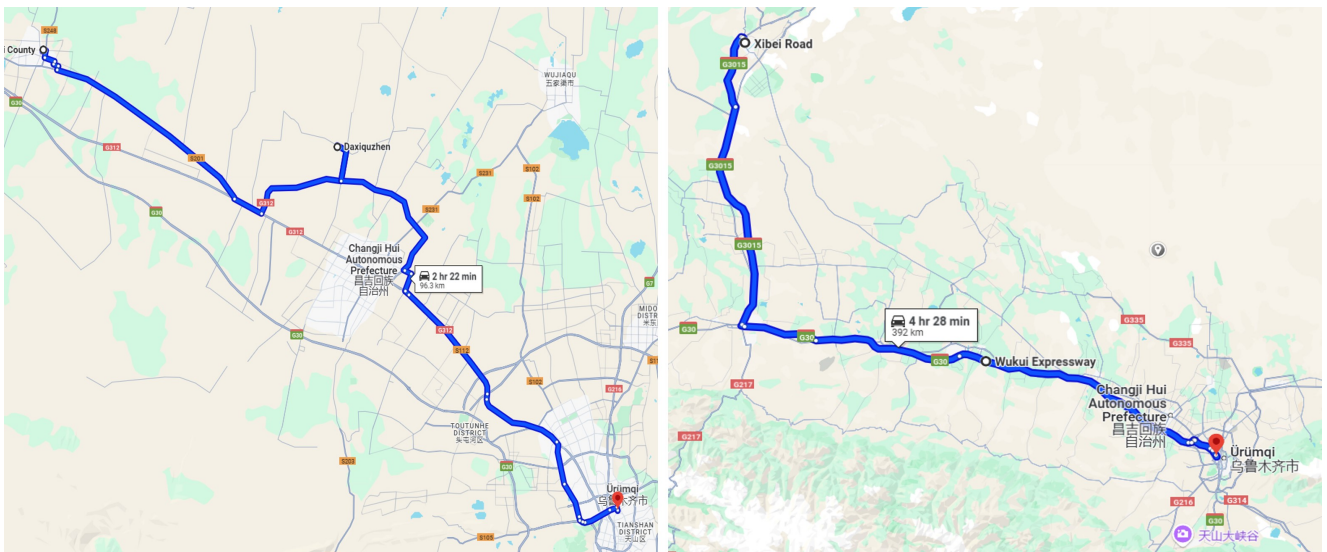


Figure 3: The routes for dataset acquisition in Urumqi, Xinjiang Autonomous Region: the left illustrates the morning of December 9, 2023, while the right depicts the evening of January 2, 2024.[33]

Table 1: Comparison Between Our Dataset and Existing Lane Detection Datasets

Dataset	Frames	Multi-traffic scenarios	Instance-level annotation	Number of foggy datasets	Resolution
Caltech-Lanes [37]	1.2k	✗	✓	None	640 x 480
Tusimple [24]	6.4k	✗	✓	None	1280 x 720
LLAMAS [38]	100k	✓	✓	None	1276 x 717
Appolloscape [39]	110k	✓	✗	None	3384 x 2710
BDD100k [40]	100k	✓	✗	None	1280 x 720
CULane [8]	133k	✓	✓	None	1640 x 590
CurveLanes [41]	150k	✓	✓	None	1280 x 720
FoggyLane (ours)	1.423k	✓	✓	1.423k	1640 x 590

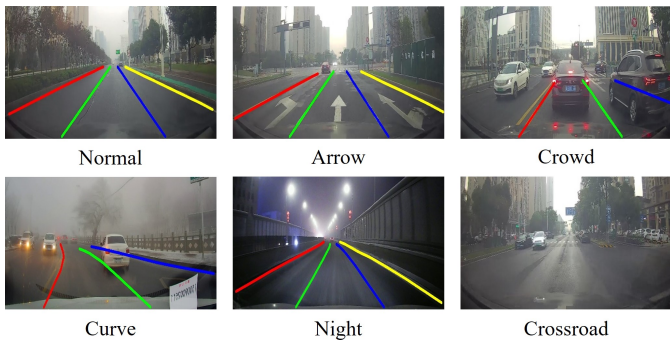


Figure 4: The different road types of FoggyLane images examples.

LLAMAS[38], lack foggy weather data. To address this, we developed FoggyLane, a dataset specifically designed for foggy conditions. Data was collected using a monocular forward-facing camera at various times and locations, including Suzhou and Urumqi, China, between October 2023 and January 2024. The dataset includes 1,086 images at various resolutions, which were resized to  $1640 \times 590$  for consistency.

Since foggy conditions are rare, we extended the dataset by incorporating foggy driving scenes from two YouTube videos[42], resulting in an additional 337 images. The final FoggyLane dataset contains 1,423 images, covering six road scenes: Normal, Arrow, Crowd, Curve, Night, and Crossroad. The dataset was partitioned into training, validation and testing sets, with stratification to maintain a consistent distribution of scene types across both subsets.

Comparing FoggyLane with existing datasets, such as Caltech-Lanes[37] and Tusimple[24], which focus on single traffic scenarios, and LLAMAS[38], which uses high-precision map annotations, we found that these datasets do not cover foggy weather scenarios. While ApolloScape [39] and BDD100k [40] include multiple traffic scenarios, they lack instance-level annotations. Similarly, although CULane [8] and CurveLanes [41] cover a wide range of traffic scenes, they do not include foggy conditions. Models trained on datasets limited to clear weather struggle in fog, where lane boundaries are blurred and image quality reduced. To fill this gap, FoggyLane offers a thorough solution for lane detection in foggy conditions with instance-level annotations.

Our dataset has two key advantages:

- 1) Pioneering foggy lane detection dataset: FoggyLane is a dataset specifically designed to address foggy weather scenarios. It covers a range of challenging conditions, including foggy congested roads, foggy curves, and foggy night roads. This dataset is crucial for testing the robustness of ADAS under adverse conditions.
- 2) Strict annotation standards: The dataset follows strict annotation guidelines, including marking the center of lanes, connecting lane markings at intersections, and prioritizing solid lines over grid lines, etc.[43]. These rigorous annotations can significantly improve the accuracy and consistency of lane detection in foggy weather, thus enhancing the stability and safety of autonomous driving systems and providing a solid data foundation for the reliable deployment of autonomous technology.

### 3.2. FoggyCULane and FoggyTusimple

Currently, numerous datasets are available for lane detection. Among them, we select two widely adopted and representative benchmarks: CULane[8] and TuSimple[24]. The CULane dataset [8] serves as an extensive and demanding benchmark, encompassing various scenarios such as highways, urban roads, and rural regions in Beijing. In contrast, the TuSimple dataset [24] primarily comprises daytime driving videos collected on American highways, featuring a variety of lighting conditions and complex traffic situations. Based on these datasets, we generate synthetic foggy versions, named FoggyCULane and FoggyTuSimple, to facilitate evaluation under adverse weather conditions.

The method for generating foggy images is inspired by the model [18], and the complete generation process is shown in Fig. 5. To be specific, the atmospheric scattering model can effectively utilize prior information to analyze the degradation mechanisms of image quality in foggy conditions. It models foggy images as a combination of scattered light and direct light based on optical principles, ultimately synthesizing a clear image into a foggy one. The mathematical modeling equation defined by Koschmieder [44] is represented as:

$$I(x) = J(x)t(x) + A(1 - t(x)) \quad (1)$$

where  $x$  indicates a certain pixel of the image,  $J(x)$  refers to the original clear image of the object and  $I(x)$  refers to the foggy

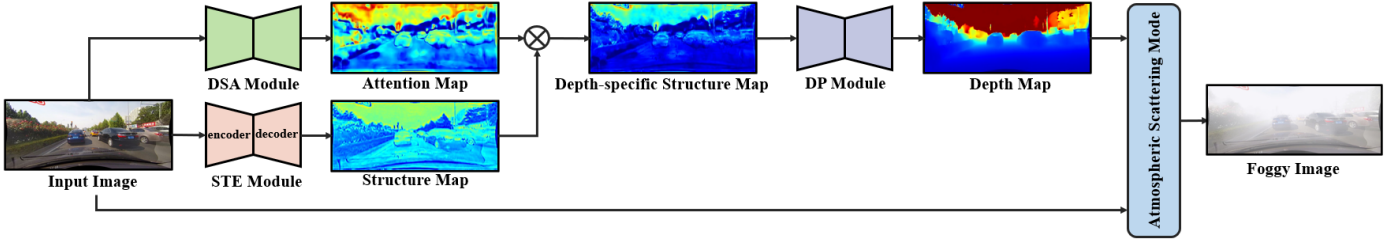


Figure 5: Networks of foggy image generation.  $\otimes$  represents element-wise multiplication.

image.  $A$  is the atmospheric light value at infinity and  $t(x)$  can be further defined as:

$$t(x) = e^{-\beta d(x)} \quad (2)$$

where  $\beta$  is the extinction coefficient, which is closely related to the concentration, size, type and distribution of particulate matter.  $d(x)$  represents the distance between the object and the viewer. As this distance increases, the transmittance decreases, resulting in thicker fog.

To calculate the corresponding  $d(x)$ , we use the S2R-DepthNet[45] that has good generalization performance across various applications. The S2R-DepthNet consists of three modules that decouple the structural and textural information of the input image. Then they suppress information irrelevant to depth and use structural information for depth prediction. The Structure Extraction Module (STE) breaks down the image to cap-

ture domain-independent structural details. The Depth-specific Attention (DSA) generates an attention map from the original image. Once processed through the DSA and STE Modules, as depicted in Fig. 5, the attention map and structural map are multiplied to produce a refined and all-encompassing depth-specific structure map. The Depth Prediction (DP) module is then responsible for estimating the depth.

According to the transmittance formula Eq. (2), we use the dark channel prior[46] to calculate the average atmospheric light value  $A$ . In the non-sky area of an outdoor clear image, there is usually at least one very small or close to zero value in the RGB image for each pixel, which is called the dark channel of that pixel. Therefore, for any image  $I$ , the mathematical formula for its corresponding dark channel image  $I_{\text{dark}}(x)$  can be



Figure 6: The FoggyCULane dataset examples. (a) is the original CULane dataset. And (b) to (d) are the foggy images of different concentrations with  $\beta$  values of 2, 4, and 8, respectively.

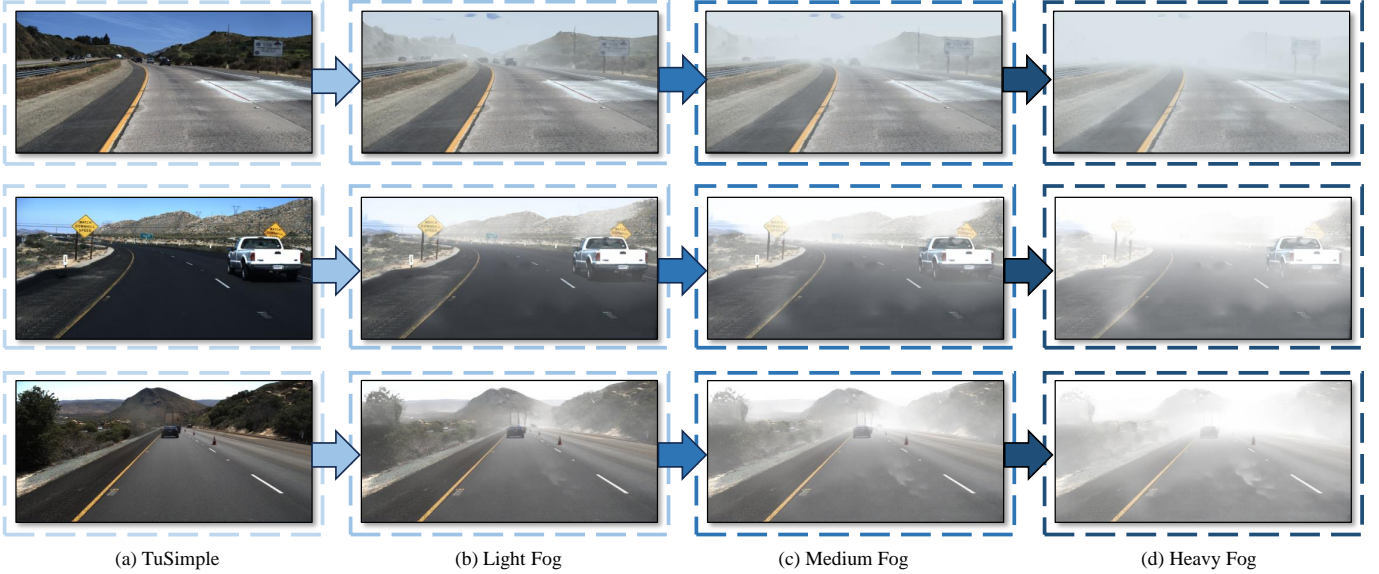


Figure 7: The FoggyTuSimple dataset examples. (a) is the original TuSimple dataset. And (b) to (d) are the foggy images of different concentrations with  $\beta$  values of 2, 4, and 8, respectively.

defined as:

$$I_{\text{dark}}(x) = \min_{c \in R, G, B} \left( \min_{y \in \omega(x)} I_c(y) \right) \quad (3)$$

where  $I_c(y)$  is the value of the  $c$ -th channel of image  $I$  at pixel point  $y$ , and  $\omega(x)$  is a small region around pixel point  $x$ . In the dark channel, find the top 0.1% brightest pixels and take the maximum value of their RGB channels as an approximation of the average atmospheric light value  $A$ . After obtaining the transmittance and the average atmospheric light value, the images of light fog, medium fog, and heavy fog can be obtained by fine-tuning the extinction coefficient  $\beta$ . The original images and the foggy images generated under different  $\beta$  values are displayed in Figs. 6 and 7.

## 4. Methods

### 4.1. Overall structure

To address the challenge of lane detection in foggy conditions, where visibility is significantly reduced, we propose a fog-enhanced lane detection network. The network works through several collaborative modules to tackle the challenges posed by foggy images, with the overall architecture shown in Fig. 8. The input image first passes through the backbone network, where feature extraction occurs, followed by the Global Feature Fusion Module (GFFM). This module is designed to mitigate the loss of global information in foggy images, allowing the network to retain essential global context. The output is a feature map enriched with both local and global information, crucial for accurate lane detection.

The multi-level feature map from the backbone is then passed into the Neck section of the network, which employs HRNetV2[47] for multi-scale feature fusion. HRNetV2 excels in integrating high-resolution and low-resolution features from different stages of the backbone. This process helps the network

capture spatial information at multiple scales, producing a rich, multi-scale feature representation that forms the basis for lane instance detection.

Next, the Instance Detection Head processes the multi-scale feature map from the Neck network, predicting dynamic convolution kernel parameters for each lane instance. These dynamic kernels are applied to the lane mask segmentation head to isolate instance-specific features. The output includes a parameter map and a heat map, crucial for identifying lane instances. This approach eliminates the need for complex post-processing, significantly enhancing detection speed and accuracy.

The output parameter map is then passed to the Kernel Feature Fusion Module (KFFM), which learns the relationships between different lane instances. The KFFM fuses these instance-specific features, improving lane localization accuracy, especially for complex or overlapping lane lines. This module ensures that the network can better identify lane instances and refine the localization of each lane.

Finally, to compensate for the loss of edge information in foggy images, the network incorporates a Low-Level Edge Enhancement Module (LEEM). This module enhances edge features using convolution operations, recovering fine details at lane boundaries. The enhanced edge features improve the network's ability to detect lane boundaries with high precision, even under challenging foggy conditions.

### 4.2. Global Feature Fusion Module

As shown in Fig. 9, to enhance global feature integration in the Swin Transformer backbone[48], we replace the final window-based attention mechanism with a standard multi-head attention mechanism (MHSA) from Vision Transformer (ViT)[49]. While ViT excels at capturing global dependencies, it suffers from high computational cost, especially at high resolutions, making it unsuitable for real-time tasks such as lane

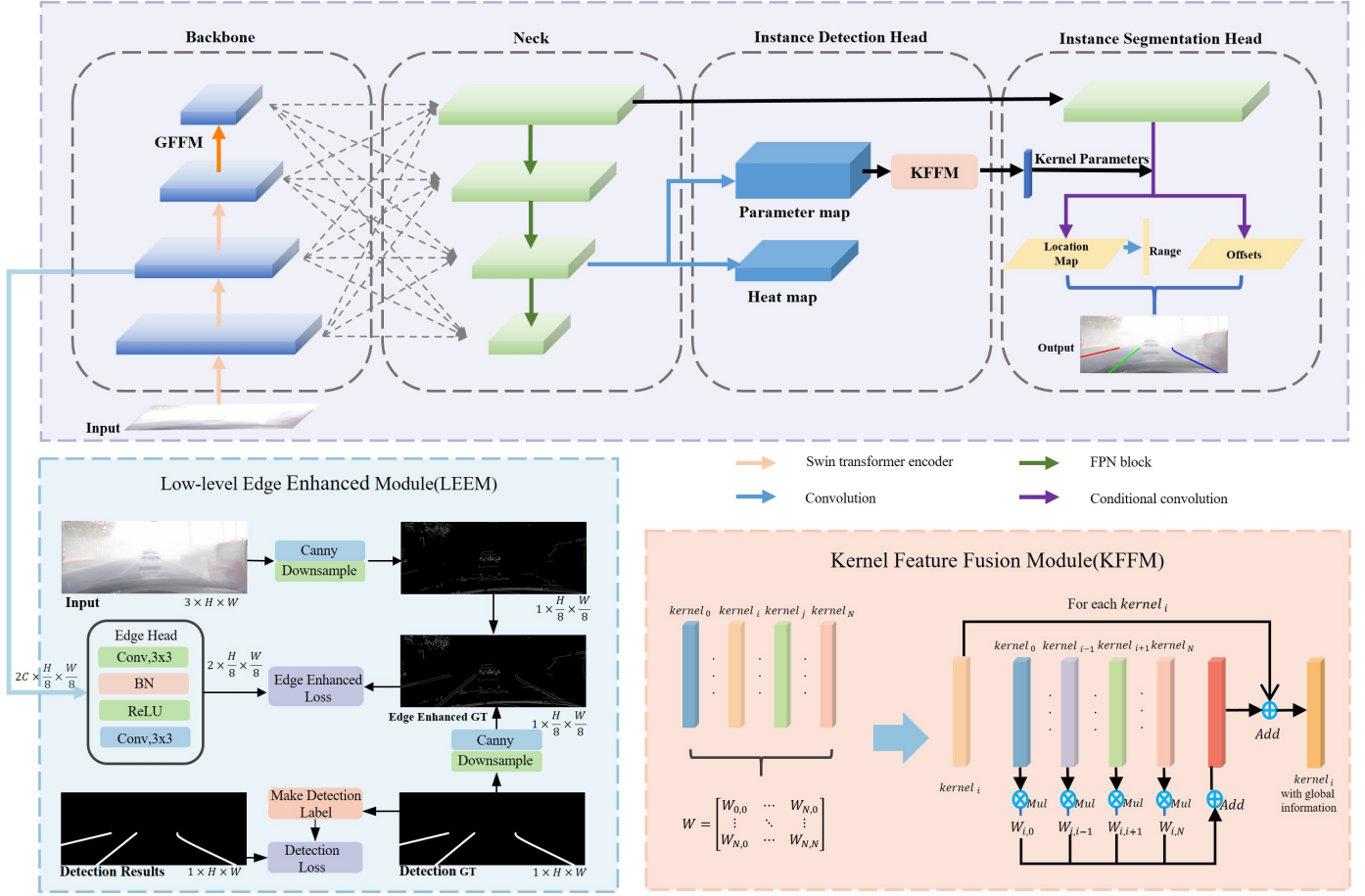


Figure 8: Overview of the proposed network.

detection. The traditional ViT computes global self-attention with a complexity of  $O(N^2)$ , where  $N$  is the number of input tokens. This high computational cost becomes prohibitive at high resolution, slowing down inference and limiting real-time processing.

In our approach, we address this issue by introducing an efficient solution: global attention is applied only after reducing the image resolution. This ensures that the computational cost of global attention is manageable, allowing us to retain the global attention mechanism of ViT while maintaining fast inference speed, which is crucial for real-time lane detection in foggy conditions.

In our design, this MHSA layer replaces the original window-based attention mechanism used in the Swin Transformer. By applying global attention after reducing the image resolution, we strike a balance between maintaining global context awareness and achieving high computational efficiency, which is crucial for real-time lane detection tasks.

### 4.3. Kernel Feature Fusion Module

Existing lane instance segmentation methods[50, 36], typically use dynamic convolution to generate kernel parameters for each instance, which improves the network’s flexibility and adaptability. However, these methods do not fully leverage the

structural relationships between lane instances, leading to limited segmentation and detection accuracy. Traditional dynamic convolution methods only consider individual lane instances and overlook the potential relationships between adjacent instances, which reduces their performance when handling complex lane scenes.

To address this limitation, we propose the Kernel Feature Fusion Module (KFFM), as shown in the bottom right of Fig. 8, which optimizes kernel generation by integrating information from adjacent lane instances. Specifically, KFFM introduces structured feature fusion into dynamic convolution, allowing each lane instance’s kernel to depend not only on the features of the current lane but also on the information from nearby lane instances. This approach enables the network to adaptively learn the relationships between lane instances, improving both detection accuracy and segmentation performance.

Let the input feature map from the lane instance detection branch be denoted as  $K = [kernel_0, kernel_1, \dots, kernel_N]$ , where each  $kernel_i \in \mathbb{R}^{k \times k \times C}$ , and define the weight matrix  $W \in \mathbb{R}^{(N+1) \times (N+1)}$  to capture the contributions of each kernel to the final fused kernel.

The final fused kernel for lane  $i$  is computed as the weighted

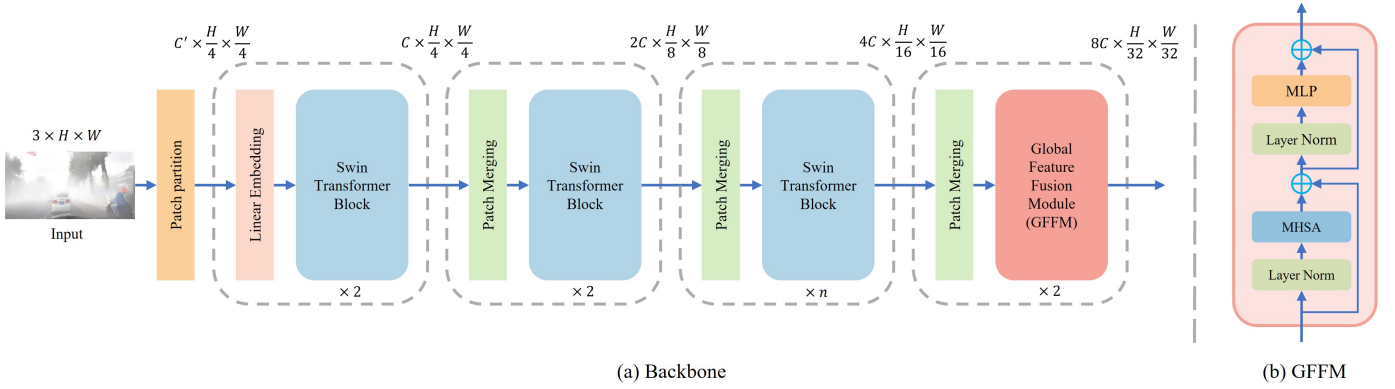


Figure 9: Backbone Network with Global Feature Fusion.

sum of the kernels:

$$\hat{kernel}_i = \sum_{j=0}^N W_{i,j} \cdot kernel_j \quad (4)$$

where  $W_{i,j}$  is the weight for the contribution of  $kernel_j$  to the fused kernel  $\hat{kernel}_i$ ; The weight matrix  $W$  is learned during training.

The final fused kernel is obtained through matrix multiplication as follows:

$$\hat{K}_i = W_i \cdot K \quad (5)$$

where  $W_i$  corresponds to the row of the weight matrix  $W$  associated with kernel  $i$ .

The resulting fused kernel  $\hat{kernel}_i$  is then used in the dynamic convolution operation for lane segmentation, leading to more accurate lane detection and segmentation.

#### 4.4. Low-level Edge Enhanced Module

Images captured in foggy conditions differ from those captured in good lighting primarily due to blurriness and low contrast, which makes the edges of objects and scene details indistinct and difficult to detect. This degradation of edge information significantly impacts the algorithm’s ability to accurately understand and recognize the scene. Edge information, beyond simply marking object boundaries, also implicitly contains structural and spatial relationships about objects, which is critical for tasks such as object detection, segmentation, and tracking. We used the Canny edge detection algorithm with identical threshold settings to process both foggy and normal images, as shown in Fig. 10. The results show that fog significantly degrades edge information, particularly lane line edges, which become nearly indiscernible. Given that lane detection relies heavily on edge information—lane positioning is typically determined by the boundary between lane edges and the road background—accurate edge detection is essential for reliable lane detection.

To address the challenges posed by foggy conditions, we propose the integration of global feature fusion within both the backbone network and detection head to enhance high-dimensional global features. Additionally, we incorporate

multi-scale fusion to aggregate detailed features from low-resolution feature maps. However, this approach alone does not fully compensate for the loss of edge details in foggy images. To resolve this issue, we introduce the Low-level Edge Enhanced Module (LEEM) into the network. LEEM focuses on edge information, effectively recovering and refining the edges that are crucial for lane detection, thus improving both the accuracy and stability of lane detection in foggy environments.

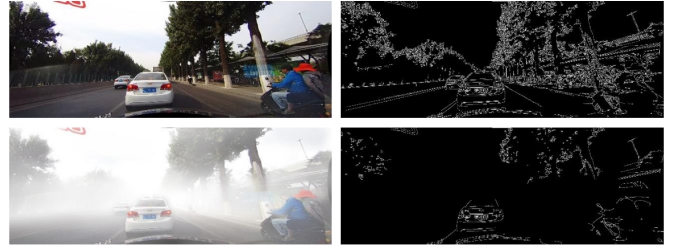


Figure 10: Comparison of edge information between foggy and normal scenarios.

LEEM works by adding an auxiliary path to the network that specifically learns edge features of the input image. The process begins with the application of the Canny operator for edge detection, followed by the reconstruction of missing lane edges using lane line labels. This ground truth for the edge enhancement module is generated by combining detected edges with labeled edges. This approach helps the network better identify lane boundaries, which are often difficult to distinguish in foggy conditions.

In the second stage of the backbone network, we introduce a branch that processes the extracted edge features. This branch sequentially applies a  $3 \times 3$  convolution followed by a  $1 \times 1$  convolution to enhance edge-related features. The mathematical representation of this process is as follows:

$$\hat{E}_{predict} = Conv_2(ReLU(BN(Conv_1(X)))) \quad (6)$$

where  $Conv_1$  is a  $3 \times 3$  convolution designed to capture spatial edge features,  $BN$  is the batch normalization layer to stabilize the learning process by normalizing the output,  $ReLU$  is the activation function that provides non-linearity,  $Conv_2$  is a  $1 \times 1$

Table 2: Comparison with Advanced Lane Detection on FoggyLane dataset.

Method	Venue	Backbone	F1@50	F1@65	F1@75	F1@85	mF1	Gflops(G)	FPS
SCNN[8]	AAAI 2018	VGG16	84.01	62.08	56.34	12.76	41.78	328.4	18.7
UFLD[35]	ECCV 2020	ResNet18	81.76	56.54	32.32	6.50	38.24	8.4	327.3
UFLD[35]	ECCV 2020	ResNet34	82.75	61.25	34.44	7.89	40.23	16.9	176.9
LaneATT[31]	CVPR 2020	ResNet18	81.98	59.61	34.78	7.69	40.06	9.3	247.7
LaneATT[31]	CVPR 2020	ResNet34	84.32	63.08	38.91	10.76	42.63	18.0	167.1
LSTR[28]	WACV 2021	ResNet34	83.79	68.23	58.29	25.32	48.91	-	124.4
RESA[25]	AAAI 2021	ResNet34	85.19	65.89	61.89	14.57	48.75	41.0	76.7
RESA[25]	AAAI 2021	ResNet50	86.24	69.22	65.27	16.55	52.34	43.0	53.0
CondLane[36]	ICCV 2021	ResNet18	90.38	75.08	47.50	47.50	10.96	10.2	194.7
CondLane[36]	ICCV 2021	ResNet34	90.58	78.45	56.48	15.59	52.25	19.6	136.5
CLRNet[16]	CVPR 2022	ResNet34	91.56	82.43	65.61	30.20	58.14	21.5	90.0
CLRNet[16]	CVPR 2022	DLA34	92.09	83.98	72.15	41.61	62.28	18.5	81.3
FLAMNet[32]	IEEE TITS 2023	ResNet34	89.94	78.90	55.32	12.96	50.99	30.1	32.0
FLAMNet[32]	IEEE TITS 2023	DLA34	91.16	82.77	64.95	24.22	56.70	21.7	31.7
DBNet[29]	IEEE TIV 2024	ResNet18	89.61	81.27	65.27	26.15	56.52	22.6	147.6
DBNet[29]	IEEE TIV 2024	ResNet34	90.02	83.44	71.66	40.51	60.94	32.1	129.0
HWLane[26]	IEEE TITS 2024	Res34	91.99	84.23	68.08	35.27	34.38	18.6	70.0
PolarRCNN[51]	IEEE TITS 2025	ResNet34	91.07	79.38	57.44	14.74	52.42	19.0	171.6
PolarRCNN[51]	IEEE TITS 2025	DLA34	90.02	83.44	71.66	40.51	51.97	16.0	150.4
Ours	-	SwinGFFM-t	92.34	84.65	70.99	35.77	60.82	12.0	70.4 / 304.7*
Ours	-	SwinGFFM-s	<b>95.04(2.95↑)</b>	<b>88.61(4.63↑)</b>	<b>77.32(5.17↑)</b>	<b>45.02(3.41↑)</b>	<b>65.60(3.32↑)</b>	20.3	38.2 / 192.9*

Note: For a fairer comparison, we re-evaluated the FPS of the source code available detectors using one NVIDIA GeForce RTX 3090 GPU on the same machine. \* indicates the FPS after acceleration with TensorRT.

convolution used to reduce the dimensionality and refine edge features.

During training, the edge information extracted via the Canny operator from both the input image and ground truth (GT) lane lines is first downsampled to match the resolution of the network’s predicted edge information  $\hat{E}_{predict}$ . Then, these two edge information maps are merged. The final combined edge information is represented as  $\hat{E}_{GT}$ , which can be computed as:

$$\hat{E}_{GT} = Edge_I + Edge_{Lane} \quad (7)$$

where  $Edge_I$  is the edge information obtained from the input image  $I$  using the Canny operator,  $Edge_{Lane}$  is the edge information derived from the lane ground truth (GT) using the Canny operator.

Next, we compute the cross-entropy loss between the predicted edge information  $\hat{E}_{predict}$  and the final combined edge information  $\hat{E}_{GT}$ . This loss function is formulated as:

$$L_{edge} = - \sum_i (e_{gt}^i \log(p_i) + (1 - e_{gt}^i) \log(1 - p_i)) \quad (8)$$

where  $e_{gt}^i$  represents the ground truth label for pixel  $i$  (1 if it’s part of the edge, 0 otherwise),  $p_i$  is the predicted probability that pixel  $i$  is part of the edge.

The LEEM module allows the network to effectively enhance critical edge details in lane detection, significantly improving both the accuracy and stability of lane detection in foggy conditions. This module not only recovers lost edge information in images but also integrates information from various sources, using the cross-entropy loss function to optimize the network. As a result, LEEM plays a key role in enhancing the robustness of lane detection systems in challenging environments.

#### 4.5. Loss functions

Based on the above, our method involves a total of five prediction tasks: lane start point prediction, row-based segmentation prediction, vertical range prediction, offset prediction, and edge prediction. The loss functions for each task are detailed below.

##### 4.5.1. Lane start point prediction

In feature maps with a large receptive field and low resolution, the lane line start point is difficult to be accurately represented by a single pixel location. Moreover, in such large receptive field feature maps, pixels near the target point exhibit similar features. If these pixels are directly labeled as negative samples, it will interfere with the network training and make it difficult for the network to learn and optimize. Therefore, this method uses a Gaussian kernel function to generate a heatmap label for the lane line start point. Each element in the heatmap label represents the confidence that the position corresponds to the target point; the closer to the target point, the higher the confidence, and the farther away, the lower the confidence. In other words, the ground truth is softly labeled with a Gaussian function, making it easier for the network to converge. Suppose  $(x, y)$  denotes a position on the low-resolution feature map, and  $(p_x, p_y)$  represents the coordinate of the target point on the low-resolution feature map. Then, the ground truth heatmap  $GT$  value at position  $(x, y)$  is defined as:

$$GT(x, y) = \exp\left(-\frac{(x - p_x)^2 + (y - p_y)^2}{2\sigma^2}\right) \quad (9)$$

where  $\sigma$  controls the decay rate of the Gaussian kernel. A larger  $\sigma$  results in slower confidence decay and thus a larger heatmap area.

This method combines the Gaussian heatmaps of all lane line start points within the image into a single heatmap. When

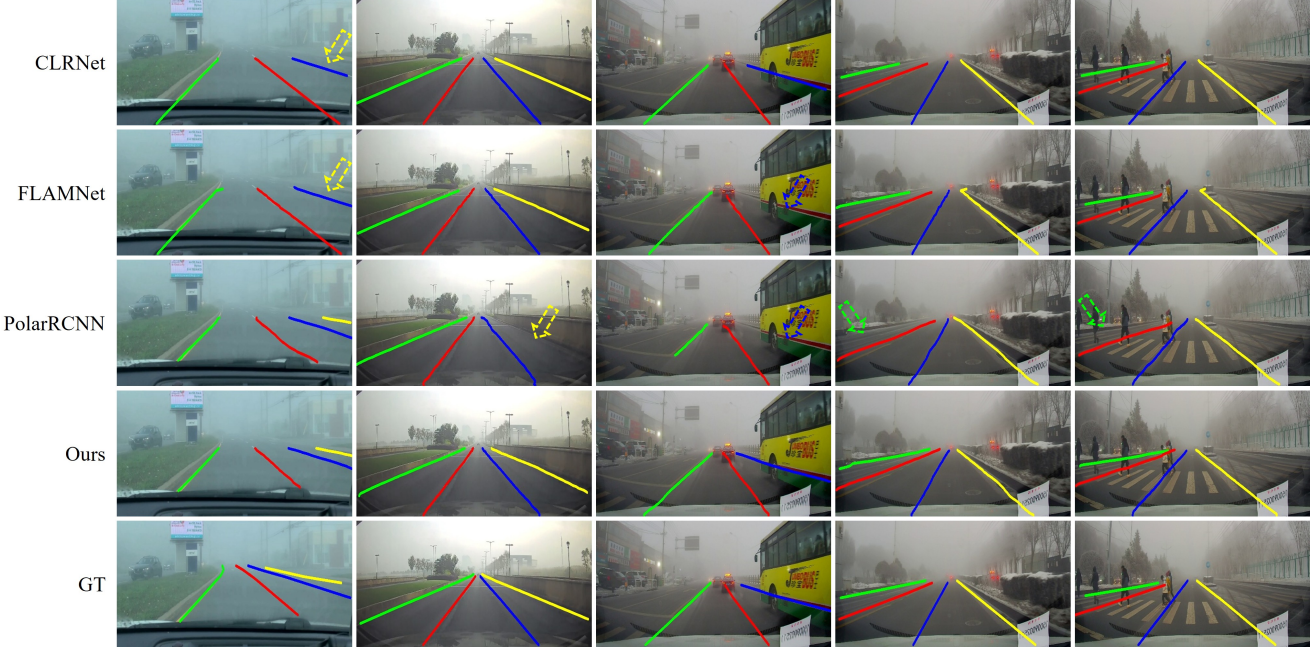


Figure 11: Visualization results of CLRNNet[16], FLAMNet[32], PolarRCNN[51] and our method on FoggyLane testing set. The arrows indicate instances of lane lines that were not correctly detected by the corresponding method.

multiple heatmaps respond at the same location, the maximum value is retained to form the final ground truth heatmap. Then, the Focal Loss is used to calculate the loss between the predicted heatmap and the ground truth heatmap. Let the predicted heatmap value at position  $(x, y)$  be  $P_{xy}$ , and let  $N$  be the total number of pixels in the heatmap. The Focal Loss between the predicted heatmap and the ground truth heatmap is defined as:

$$\mathcal{L}_{hm} = -\frac{1}{N} \sum_{x,y} \begin{cases} (1 - P_{xy})^\alpha \log(P_{xy}), & \text{if } GT(x, y) = 1 \\ (1 - GT(x, y))^\beta (P_{xy})^\alpha \log(1 - P_{xy}), & \text{otherwise} \end{cases} \quad (10)$$

#### 4.5.2. Row-based segmentation prediction

Row-based segmentation predicts a horizontal coordinate  $E(\hat{x}_i)$  for each row. For this task, our method uses the L1 loss function to optimize the predicted coordinates. Suppose  $V$  denotes the effective vertical range of the lane line,  $N_v$  is the number of effective rows, and  $x_i$  is the ground truth horizontal coordinate. The loss function is defined as:

$$L_{row} = \frac{1}{N_v} \sum_{i \in V} |E(\hat{x}_i) - x_i| \quad (11)$$

#### 4.5.3. Vertical range prediction

For the label of the lane line vertical range vector prediction, our method uses a  $1 \times Y$  vector representation. If the lane line passes through the  $Y_i$  row, its value is 1; otherwise, it is 0. Thus, this can be regarded as a segmentation task. Our method optimizes it using the cross-entropy loss function. Suppose  $v_i$  denotes the predicted probability that the  $i$ -th row is positive, then the loss function is defined as:

$$L_{range} = \sum (-y_{gt}^i \log(v_i) - (1 - y_{gt}^i) \log(1 - v_i)) \quad (12)$$

#### 4.5.4. Offset prediction

Firstly, the generation of ground truth labels for offset prediction is required. For each lane line, the proposed method constructs the ground truth offset as the horizontal displacement relative to the lane centerline for each grid cell within a specified width. The predicted offsets are optimized using an L1 loss function. Let  $\delta_{xy}$  denote the ground truth offset at coordinate  $(x, y)$ ,  $\hat{\delta}_{xy}$  the predicted offset, and  $\Omega$  the region surrounding the lane line. The loss function is then formulated as follows:

$$L_{offset} = \frac{1}{N_\Omega} \sum_{(x,y) \in \Omega} |\hat{\delta}_{xy} - \delta_{xy}| \quad (13)$$

#### 4.5.5. Edge prediction

For the task of edge enhancement, the method treats it as an edge segmentation problem, which is essentially a binary classification task. The labels at edge locations are assigned a value of 1, while non-edge locations are assigned 0. Accordingly, the cross-entropy loss function is employed for optimization.

As discussed in Section 4.4, the loss function for edge prediction is defined as:

$$L_{edge} = \sum_i (-e_{gt}^i \log(p_i) - (1 - e_{gt}^i) \log(1 - p_i)) \quad (14)$$

where  $e_{gt}^i$  denotes the label of pixel  $i$ , and  $p_i$  represents the predicted probability of the pixel being part of the edge.

#### 4.5.6. Total loss

To balance the influence of different tasks on the overall training of the network, a weighted fusion of the loss functions for each sub-task is employed. The total loss function is formulated as follows:

Table 3: Comparison with Advanced Lane Detection on FoggyCULane dataset

Method	Venue	Backbone	Normal	Crowded	Dazzle light	Shadow	No line	Arrow	Curve	Cross	Night	Total
SCNN[8]	AAAI 2018	VGG16	91.07	71.32	67.23	65.23	49.14	88.06	67.07	1344	70.78	72.94
UFLD[35]	ECCV 2020	ResNet18	87.57	65.47	55.21	60.38	38.66	82.26	57.29	1849	60.61	67.69
UFLD[35]	ECCV 2020	ResNet34	89.10	68.29	60.91	62.03	41.98	85.17	63.88	2371	70.13	70.13
LaneATT[31]	CVPR 2020	ResNet18	90.52	71.52	65.70	68.92	47.31	86.32	62.34	870	67.64	74.30
LaneATT[31]	CVPR 2020	ResNet34	91.68	72.93	67.23	65.23	49.14	88.06	67.07	1344	70.78	75.53
LSTR[28]	WACV 2021	ResNet34	85.79	63.45	56.73	58.72	38.20	79.31	55.34	1068	57.62	65.64
RESA[25]	AAAI 2021	ResNet34	90.97	72.32	67.31	74.01	46.52	86.32	65.26	1536	73.62	74.97
RESA[25]	AAAI 2021	ResNet50	92.09	73.49	67.40	73.87	47.92	87.48	69.28	1722	69.85	75.19
CondLane[36]	ICCV 2021	ResNet18	91.56	74.41	71.12	77.89	48.59	86.73	71.34	1262	71.00	76.46
CondLane[36]	ICCV 2021	ResNet34	91.76	75.55	69.62	74.62	50.01	87.40	71.29	1427	72.11	77.06
CLRNet[16]	CVPR 2022	ResNet34	92.96	76.32	73.40	79.06	51.46	89.39	71.83	1301	73.64	78.36
CLRNet[16]	CVPR 2022	DLA34	93.23	77.64	73.90	79.23	52.11	89.45	72.48	1109	73.63	79.04
FLAMNet[32]	IEEE TITS 2023	ResNet34	92.60	76.61	71.42	79.81	50.89	89.04	71.47	1073	74.17	78.45
FLAMNet[32]	IEEE TITS 2023	DLA34	92.98	77.26	71.84	79.76	51.29	89.34	71.38	1143	73.93	78.77
DBNet[29]	IEEE TIV 2024	ResNet18	84.91	69.27	60.86	67.94	45.69	79.04	67.50	1045	68.57	71.33
DBNet[29]	IEEE TIV 2024	ResNet34	85.61	69.35	61.22	66.50	45.73	79.19	66.51	<b>837</b>	69.93	71.87
HWLane[26]	IEEE TITS 2024	Res34	90.85	73.32	67.18	75.32	47.18	87.14	63.38	1456	69.20	74.61
PolarRCNN[51]	IEEE TITS 2025	ResNet34	93.34	77.76	<b>75.26</b>	79.76	53.25	89.62	<b>75.94</b>	1289	74.54	78.68
PolarRCNN[51]	IEEE TITS 2025	DLA34	92.90	77.50	74.03	80.89	51.71	89.76	<b>73.02</b>	1226	74.21	79.13
Ours	-	SwinGFFM-t	92.68	77.50	71.52	80.42	50.95	88.92	72.08	950	73.11	78.66
Ours	-	SwinGFFM-s	<b>93.40(0.07↑)</b>	<b>78.63(0.87↑)</b>	73.89	<b>82.74(1.85↑)</b>	<b>53.75(0.50↑)</b>	<b>89.82(0.37↑)</b>	74.09	1146	<b>74.97(0.76↑)</b>	<b>79.85(0.72↑)</b>

Note: Our method attains state-of-the-art (SOTA) results in multiple scenarios including Normal, Crowded, Shadow, No-line, Arrow and Night conditions, as well as in the overall (Total) performance.

$$L_{\text{total}} = \alpha L_{\text{hm}} + \beta L_{\text{row}} + \gamma L_{\text{range}} + \delta L_{\text{offset}} + \varepsilon L_{\text{edge}} \quad (15)$$

where the network achieves optimal performance when the weights are set as  $\alpha = 1$ ,  $\beta = 1$ ,  $\gamma = 1$ ,  $\delta = 0.4$ , and  $\varepsilon = 0.1$ .

## 5. Experiments

### 5.1. Datasets

In the Data Construction chapter, we introduce the FoggyLane dataset, which was constructed from real-world collections for foggy lane detection, along with the FoggyCULane and FoggyTusimple datasets that were synthesized through modeling foggy images. Our method is evaluated on these three datasets.

FoggyLane is a lane detection dataset specifically designed for foggy scenarios, containing 1,423 frames of foggy lane images for training and testing. All images are of resolution 1640x590 pixels.

FoggyCULane is synthesized from the large-scale challenging lane detection dataset CULane using a foggy image modeling approach. It maintains the same number of images as CULane. The resolution of all images is also 1640x590 pixels.

FoggyTusimple is synthesized from Tusimple through the foggy image modeling method. At the same time, the dataset follows the same structure as Tusimple, comprising 3,268 training images, 358 validation samples, and 2,782 test cases. All visual data maintains a consistent resolution of 1280x720 pixels.

### 5.2. Evaluation Metric

Lane detection is typically approached as a semantic segmentation problem, assessed using common metrics. However, due to its distinct characteristics, lane detection also requires specialized evaluation metrics. Adhering to SCNN’s [8] framework, we link labeled or predicted lane points to form line

segments and extend them into 30-pixel-wide regions. Subsequently, we compute the Intersection over Union (IoU), and if the IoU value exceeds a predefined threshold, typically set at 0.5, the prediction is considered correct. From this, we calculate Precision, Recall, and F1-score using the following formulas:

$$F1 = \frac{2 \times \text{Precision} \times \text{Recall}}{\text{Precision} + \text{Recall}} \quad (16)$$

$$\text{Precision} = \frac{TP}{TP + FP} \quad (17)$$

$$\text{Recall} = \frac{TP}{TP + FN} \quad (18)$$

For the FoggyTusimple dataset, we use the same evaluation metrics as the Tusimple dataset. The official Tusimple dataset includes three standard metrics: false positive rate (FPR), false negative rate (FNR), and accuracy. The formula for calculating accuracy is as follows:

$$\text{Accuracy} = \frac{\sum_{clip} C_{clip}}{\sum_{clip} S_{clip}} \quad (19)$$

where  $C_{clip}$  represents the number of correctly predicted lane points in the image, while  $S_{clip}$  denotes the total number of ground truth lane points.

### 5.3. Implementation Details

We conducted experiments on the NVIDIA GeForce RTX 3090 platform. The SwinGFFM backbone network was pre-trained on the COCO dataset for 500 epochs. During lane detection training, we loaded the pre-trained weights and resized input images to  $800 \times 320$ . Various data augmentation techniques, including rotation, flipping, brightness adjustment, and

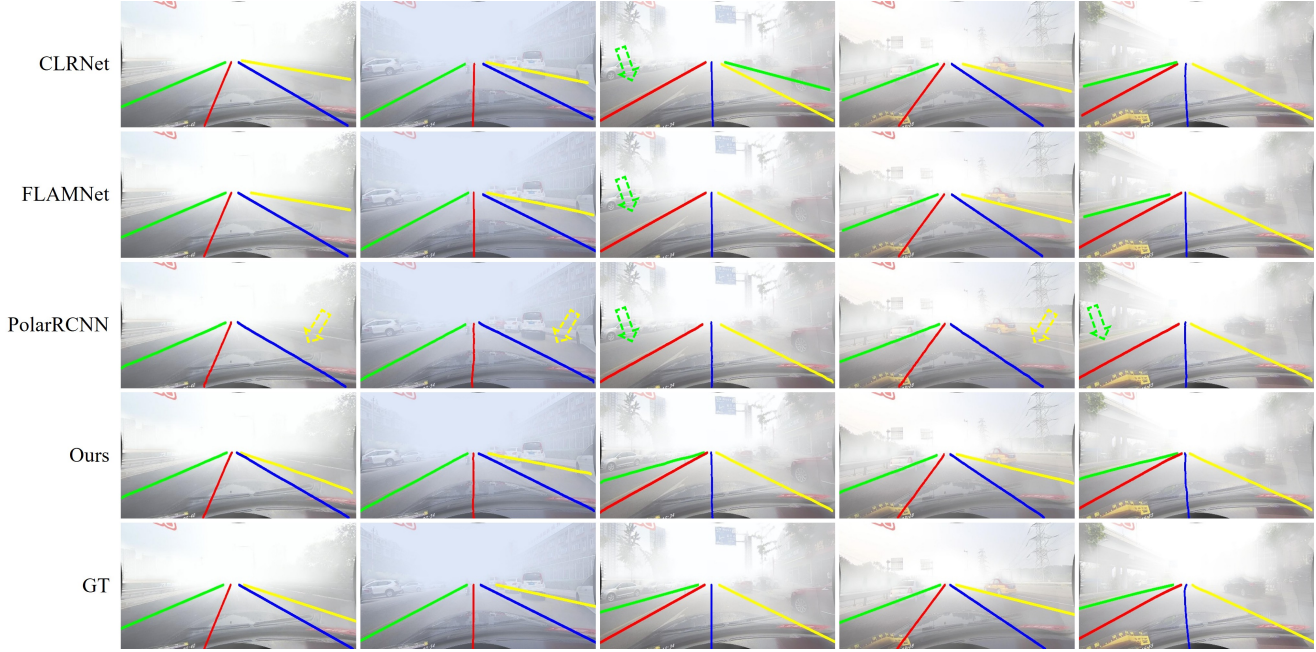


Figure 12: Visualization results of CLRNet[16], FLAMNet[32], PolarRCNN[51] and our method on FoggyCULane testing set. The arrows indicate instances of lane lines that were not correctly detected by the corresponding method.

random scaling, were applied. For full network parameters and training details, please refer to our open-source code.

To benchmark against existing methods[8, 35, 36, 25, 31, 28, 16, 32, 29, 51], we followed the training settings provided in the respective papers. For FoggyCULane and FoggyTusimple, we adopted the training parameters from the original CULane and Tusimple datasets, while for FoggyLane, we extended the training epochs to ensure reliable results

## 5.4. Quantitative Results

### 5.4.1. Results on FoggyLane

We evaluated our proposed method on the FoggyLane dataset and compared it with other leading lane detection methods. As shown in the Table 2, we mainly compared the methods in terms of F1 scores, computational complexity (GFlops), processing speed (FPS).

From the Table 2, it is evident that our method achieves state-of-the-art performance on the foggy lane detection dataset FoggyLane, with F1@50, F1@65, F1@75, and F1@85 scores of 95.04, 88.61, 77.32, and 45.02, respectively. These results surpass the best-performing alternative methods by margins of 2.95%, 4.63%, 5.17%, and 3.41%. The mean F1 (mF1) score demonstrates a 3.32% improvement over the strongest competing approach. Notably, the SwinGFFM-t variant achieves an F1@50 score of 92.34, which even exceeds the performance of DLA34-based CLRNet, previously the top-performing method among comparative approaches.

### 5.4.2. Results on FoggyCULane

We compared our method with other advanced lane detection methods on the FoggyCULane dataset. As shown in the Table 3, our method consistently achieved the best performance

across various scenarios. Additionally, our model achieved the highest overall F1 score of 79.85, which achieves a 0.72% improvement over the best alternative method.

### 5.4.3. Results on FoggyTusimple

As shown in the Table 4, the traffic scenes in the FoggyTusimple dataset are relatively simple, resulting in smaller performance differences between methods. Nonetheless, our method achieved an F1 score of 96.95, outperforming the best existing method by 0.43%. This further demonstrates the effectiveness of our method in foggy conditions.

## 5.5. Ablation Study

We conducted ablation studies on the FoggyLane and FoggyCULane datasets to evaluate the effectiveness of the GFFM, KFFM, and LEEM modules, using Swin-t as the backbone. As shown in Tables 5 and 6, each module improves the model’s performance. The GFFM module contributes the most, increasing the F1-score by 1.07 on FoggyLane and 0.41 on FoggyCULane, highlighting its ability to capture both local and global information. Adding the KFFM module further boosts the F1-score by 0.63 on FoggyLane and 0.26 on FoggyCULane. Finally, the LEEM module improves edge detection, increasing the F1-score by 0.28 on FoggyLane and 0.14 on FoggyCULane.

## 5.6. Model deployment

To further evaluate the performance of our algorithm in real-world scenarios, in addition to experiments on existing datasets, we also deployed and tested the model on the vehicle. Specifically, we implemented an edge computing system on the vehicle, as illustrated in the Fig. 14. This system comprises the

Table 4: Comparison with Advanced Lane Detection on FoggyTusimple dataset.

Method	Venue	Backbone	F1(%)	ACC(%)	FP(%)	FN(%)
SCNN[8]	AAAI 2018	VGG16	94.64	95.89	5.87	4.78
UFLD[35]	ECCV 2020	ResNet18	94.57	93.60	3.49	7.59
UFLD[35]	ECCV 2020	ResNet34	95.05	95.10	4.84	5.08
LaneATT[31]	CVPR 2020	ResNet18	95.77	95.78	3.83	3.53
LaneATT[31]	CVPR 2020	ResNet34	96.15	95.50	4.59	3.06
LSTR[28]	WACV 2021	ResNet34	94.70	95.58	5.74	4.81
RESA[25]	AAAI 2021	ResNet34	95.22	95.60	4.63	4.95
RESA[25]	AAAI 2021	ResNet50	95.51	95.83	4.53	4.43
CondLane[36]	ICCV 2021	ResNet18	95.41	94.81	3.80	5.46
CondLane[36]	ICCV 2021	ResNet34	95.65	94.69	3.63	5.13
CLRNet[16]	CVPR 2022	ResNet18	96.48	95.64	3.89	3.11
CLRNet[16]	CVPR 2022	ResNet34	96.23	95.94	4.34	3.17
FLAMNet[32]	IEEE TITS 2023	ResNet18	96.52	95.65	3.84	3.09
FLAMNet[32]	IEEE TITS 2023	ResNet101	96.34	95.98	4.45	<b>2.82</b>
DBNet[29]	IEEE TIV 2024	ResNet18	95.71	93.89	3.53	5.12
DBNet[29]	IEEE TIV 2024	ResNet34	95.61	93.72	3.48	5.38
HWLane[26]	IEEE TITS 2024	Res34	95.54	95.91	4.32	4.60
PolarRCNN[51]	IEEE TITS 2025	ResNet34	96.33	95.91	4.50	2.77
PolarRCNN[51]	IEEE TITS 2025	DLA34	96.37	94.99	3.21	4.09
Ours	-	SwinGFFM-t	96.63	95.86	2.77	4.04
Ours	-	SwinGFFM-s	<b>96.95(0.43↑)</b>	<b>96.10(0.12↑)</b>	<b>2.32(0.89↓)</b>	3.83

Table 5: Ablation experiments of different components on the FoggyLane dataset.

Model	GFFM	KFFM	LEEM	F1-score	Gflops(G)
Baseline				90.36	13.77
	✓			91.43	11.94
	✓	✓		92.06	11.97
<b>Ours</b>	✓	✓	✓	<b>92.34↑</b>	12.01

NVIDIA Jetson AGX Orin edge computing device, a monitor, a camera, and a power supply unit. The results of the evaluation demonstrate that our approach can operate in real-time with high accuracy on the vehicle’s edge computing platform, despite the constraints on computational resources.

Table 6: Ablation experiments of different components on the FoggyCULane dataset.

Model	GFFM	KFFM	LEEM	F1-score	Gflops(G)
Baseline				77.85	13.77
	✓			78.26	11.94
	✓	✓		78.52	11.97
<b>Ours</b>	✓	✓	✓	<b>78.66↑</b>	12.01

## 6. Conclusion

This study focuses on lane detection in foggy conditions, aiming to address the range of challenges posed by foggy environments, which is crucial for ensuring driving safety in fog and enhancing Advanced Driver Assistance System (ADAS) capabilities. To address the current lack of publicly available datasets for lane detection in foggy conditions, we constructed a real-world foggy lane dataset, FoggyLane, and synthesized two additional foggy datasets, FoggyCULane and FoggyTusimple, based on the popular CULane and Tusimple datasets.

In response to the challenges of lane detection in foggy scenarios, we propose an end-to-end fog-enhanced lane detection method. First, this method incorporates a Global Feature Fusion Module in the backbone network to address the absence of global spatial information in foggy scenes. Second, we employ a dynamic convolution-based detection head for instance-sensitive lane segmentation, integrating a Kernel Feature Fusion Module within the detection head to automatically capture associations between lane instances. Additionally, a Low-Level Edge Enhancement Module was added to increase the network’s focus on edge information, mitigating the loss of edge details and improving lane detection accuracy under foggy conditions.

Comparative experiments on the FoggyLane, FoggyCULane, and FoggyTusimple datasets with other advanced lane detection methods demonstrate that our approach achieves superior performance in both clear and foggy conditions, significantly improving lane detection accuracy. Furthermore, with TensorRT acceleration, our method achieves an inference speed of 38.4 FPS on the NVIDIA Jetson AGX Orin, further validating its practical applicability in real-world scenarios.

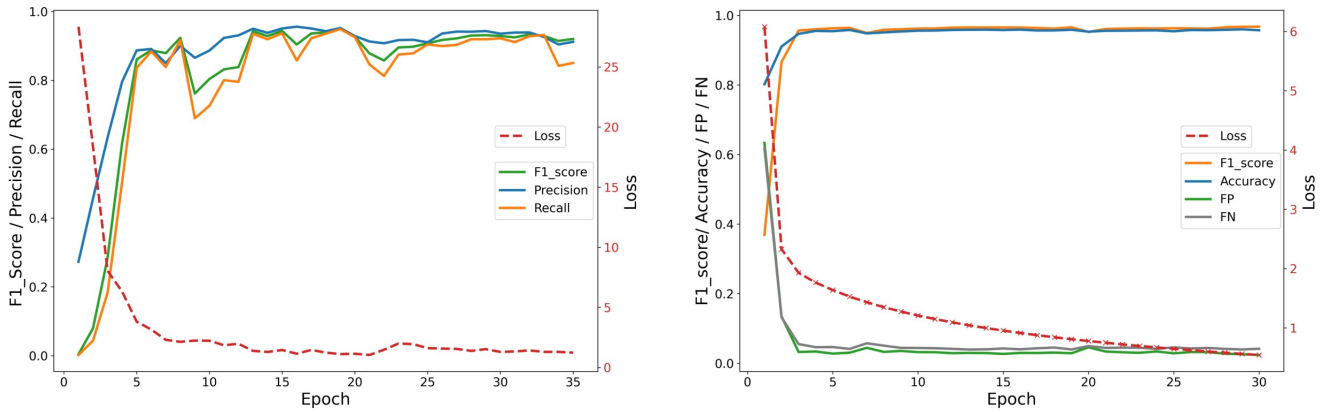


Figure 13: Several metrics of our model’s performance during the training process on the FoggyLane and FoggyTusimple datasets, with results on FoggyLane on the left and FoggyTusimple on the right.



Figure 14: A edge computing system built with NVIDIA Jetson AGX Orin. After experimental validation, it has been demonstrated that our method can run accurately on the vehicle’s edge computing platform with limited computational resources, achieving a performance of 38.4 FPS.

## Acknowledgement

This project is jointly supported by National Natural Science Foundation of China (Nos. 52172350, W2421069 and 51775565), the Guangdong Basic and Applied Research Foundation (No. 2022B1515120072), the Guangzhou Science and Technology Plan Project (No. 2024B01W0079), the Science and Technology Planning Project of Guangdong Province (No. 2023B1212060029). **We would like to release our source code and dataset.**

## References

[1] L.-H. Wen, K.-H. Jo, Deep learning-based perception systems for autonomous driving: A comprehensive survey, *Neurocomputing* 489 (2022) 255–270. doi:<https://doi.org/10.1016/j.neucom.2021.08.155>.

[2] X. Luo, Y. Huang, J. Cui, K. Zheng, Deep learning-based lane detection for intelligent driving: A comprehensive survey of methods, datasets, challenges and out-

looks, *Neurocomputing* 650 (2025) 130795. doi:<https://doi.org/10.1016/j.neucom.2025.130795>.

[3] Pexels, <https://www.pexels.com/zh-cn/> (2025).

[4] J. Son, H. Yoo, S. Kim, K. Sohn, Real-time illumination invariant lane detection for lane departure warning system, *Expert Systems with Applications* 42 (4) (2015) 1816–1824. doi:<https://doi.org/10.1016/j.eswa.2014.10.024>.

[5] C. Hou, J. Hou, C. Yu, An efficient lane markings detection and tracking method based on vanishing point constraints, in: *Chinese Control Conference (CCC)*, IEEE, 2016, pp. 6999–7004. doi:[10.1109/ChiCC.2016.7554460](https://doi.org/10.1109/ChiCC.2016.7554460).

[6] D. Neven, B. De Brabandere, S. Georgoulis, M. Proesmans, L. Van Gool, Towards end-to-end lane detection: an instance segmentation approach, in: *2018 IEEE Intelligent Vehicles Symposium (IV)*, IEEE, 2018, pp. 286–291. doi:[10.1109/IVS.2018.8500547](https://doi.org/10.1109/IVS.2018.8500547).

- [7] F. Yu, D. Wang, E. Shelhamer, T. Darrell, Deep layer aggregation, in: Proceedings of the IEEE Conference on Computer Vision and Pattern Recognition, 2018, pp. 2403–2412. doi:10.1109/CVPR.2018.00255.
- [8] X. Pan, J. Shi, P. Luo, X. Wang, X. Tang, Spatial as deep: Spatial cnn for traffic scene understanding, in: Proceedings of the AAAI Conference on Artificial Intelligence, Vol. 32, 2018.
- [9] Z. Zhao, Q. Wang, X. Li, Deep reinforcement learning based lane detection and localization, Neurocomputing 413 (2020) 328–338. doi:https://doi.org/10.1016/j.neucom.2020.06.094.
- [10] J. Li, F. Jiang, J. Yang, B. Kong, M. Gogate, K. Dashtipour, A. Hussain, Lane-deeplab: Lane semantic segmentation in automatic driving scenarios for high-definition maps, Neurocomputing 465 (2021) 15–25. doi:https://doi.org/10.1016/j.neucom.2021.08.105.
- [11] H. Abualsaud, S. Liu, D. B. Lu, K. Situ, A. Rangesh, M. M. Trivedi, Laneaf: Robust multi-lane detection with affinity fields, IEEE Robotics and Automation Letters 6 (4) (2021) 7477–7484. doi:10.1109/LRA.2021.3098066.
- [12] J. Redmon, You only look once: Unified, real-time object detection, in: Proceedings of the IEEE Conference on Computer Vision and Pattern Recognition, 2016, pp. 779–788. doi:10.1109/CVPR.2016.91.
- [13] A. Farhadi, J. Redmon, Yolov3: An incremental improvement, arXiv preprint arXiv:1804.02767 (2018) 1–6doi:10.48550/arXiv.1804.02767.
- [14] Y. Tian, J. Gelernter, X. Wang, W. Chen, J. Gao, Y. Zhang, X. Li, Lane marking detection via deep convolutional neural network, Neurocomputing 280 (2018) 46–55. doi:https://doi.org/10.1016/j.neucom.2017.09.098.
- [15] Z. Chen, Q. Liu, C. Lian, Pointlanenet: Efficient end-to-end cnns for accurate real-time lane detection, in: 2019 IEEE Intelligent Vehicles Symposium (IV), 2019, pp. 2563–2568. doi:10.1109/IVS.2019.8813778.
- [16] T. Zheng, Y. Huang, Y. Liu, W. Tang, Z. Yang, D. Cai, X. He, Clrnet: Cross layer refinement network for lane detection, in: Proceedings of the IEEE/CVF Conference on Computer Vision and Pattern Recognition, 2022, pp. 898–907. doi:10.1109/CVPR52688.2022.00097.
- [17] S.-C. Huang, T.-H. Le, D.-W. Jaw, Dsnet: Joint semantic learning for object detection in inclement weather conditions, IEEE Transactions on Pattern Analysis and Machine Intelligence 43 (8) (2020) 2623–2633. doi:10.1109/TPAMI.2020.2977911.
- [18] X. Nie, Z. Xu, W. Zhang, X. Dong, N. Liu, Y. Chen, Foggy lane dataset synthesized from monocular images for lane detection algorithms, Sensors 22 (14) (2022) 5210. doi:10.3390/s22145210.
- [19] Y. Chen, W. Li, C. Sakaridis, D. Dai, L. Van Gool, Domain adaptive faster r-cnn for object detection in the wild, in: Proceedings of the IEEE Conference on Computer Vision and Pattern Recognition, 2018, pp. 3339–3348. doi:10.1109/CVPR.2018.00352.
- [20] S. Zhang, H. Tuo, J. Hu, Z. Jing, Domain adaptive yolo for one-stage cross-domain detection, in: Asian Conference on Machine Learning, PMLR, 2021, pp. 785–797.
- [21] M. Hnewa, H. Radha, Multiscale domain adaptive yolo for cross-domain object detection, in: Proceedings of the IEEE International Conference on Image Processing, 2021, pp. 3323–3327. doi:10.1109/ICIP42928.2021.9506039.
- [22] J. Iqbal, R. Hafiz, M. Ali, Fogadapt: Self-supervised domain adaptation for semantic segmentation of foggy images, Neurocomputing 501 (2022) 844–856. doi:https://doi.org/10.1016/j.neucom.2022.05.086.
- [23] J. Li, R. Xu, J. Ma, Q. Zou, J. Ma, H. Yu, Domain adaptive object detection for autonomous driving under foggy weather, in: Proceedings of the IEEE/CVF Winter Conference on Applications of Computer Vision, 2023, pp. 612–622.
- [24] Tusimple, <https://github.com/TuSimple/tusimple-benchmark> (2017).
- [25] T. Zheng, H. Fang, Y. Zhang, W. Tang, Z. Yang, H. Liu, D. Cai, Resa: Recurrent feature-shift aggregator for lane detection, in: Proceedings of the AAAI Conference on Artificial Intelligence, Vol. 35, 2021, pp. 3547–3554. doi:10.1609/aaai.v35i4.16469.
- [26] J. Zhao, Z. Qiu, H. Hu, S. Sun, Hwlane: Hw-transformer for lane detection, IEEE Transactions on Intelligent Transportation Systems 25 (8) (2024) 9321–9331. doi:10.1109/TITS.2024.3386531.
- [27] L. Tabelini, R. Berriel, T. M. Paixao, C. Badue, A. F. De Souza, T. Oliveira-Santos, Polylanenet: Lane estimation via deep polynomial regression, in: Proceedings of the IEEE International Conference on Pattern Recognition, IEEE, 2021, pp. 6150–6156. doi:10.1109/ICPR48806.2021.9412265.
- [28] R. Liu, Z. Yuan, T. Liu, Z. Xiong, End-to-end lane shape prediction with transformers, in: Proceedings of the IEEE/CVF Winter Conference on Applications of Computer Vision, 2021, pp. 3694–3702. doi:10.1109/WACV48630.2021.00374.

- [29] X. Dai, J. Xie, G. Zhang, K. Chang, F. Chen, Z. Wang, C. Tang, Dbnet: A curve-based dynamic association framework for lane detection, *IEEE Transactions on Intelligent Vehicles* (2024). doi:10.1109/TIV.2024.3370213.
- [30] X. Li, J. Li, X. Hu, J. Yang, Line-cnn: End-to-end traffic line detection with line proposal unit, *IEEE Transactions on Intelligent Transportation Systems* 21 (1) (2019) 248–258. doi:10.1109/TITS.2019.2890870.
- [31] L. Tabelini, R. Berriel, T. M. Paixao, C. Badue, A. F. De Souza, T. Oliveira-Santos, Keep your eyes on the lane: Real-time attention-guided lane detection, in: *Proceedings of the IEEE/CVF Conference on Computer Vision and Pattern Recognition*, 2021, pp. 294–302. doi:10.1109/CVPR46437.2021.00036.
- [32] H. Ran, Y. Yin, F. Huang, X. Bao, Flamnet: A flexible line anchor mechanism network for lane detection, *IEEE Transactions on Intelligent Transportation Systems* 24 (2023) 12767–12778. doi:doi:10.1109/TITS.2023.3290991.
- [33] GoogleMaps, <https://www.google.com/maps> (Accessed: 2024).
- [34] S. Yoo, H. S. Lee, H. Myeong, S. Yun, H. Park, J. Cho, D. H. Kim, End-to-end lane marker detection via row-wise classification, in: *Proceedings of the IEEE/CVF Conference on Computer Vision and Pattern Recognition Workshops*, 2020, pp. 1006–1007. doi:10.1109/CVPRW50498.2020.00511.
- [35] Z. Qin, H. Wang, X. Li, Ultra fast structure-aware deep lane detection, in: *European Conference on Computer Vision*, Springer, 2020, pp. 276–291. doi:10.1007/978-3-030-58586-0\_17.
- [36] L. Liu, X. Chen, S. Zhu, P. Tan, Conclanenet: a top-to-down lane detection framework based on conditional convolution, in: *Proceedings of the IEEE/CVF International Conference on Computer Vision*, 2021, pp. 3773–3782. doi:10.1109/ICCV48922.2021.00375.
- [37] M. Aly, Real time detection of lane markers in urban streets, in: *2008 IEEE Intelligent Vehicles Symposium (IV)*, 2008, pp. 7–12. doi:10.1109/IVS.2008.4621152.
- [38] K. Behrendt, R. Soussan, Unsupervised labeled lane markers using maps, in: *Proceedings of the IEEE/CVF International Conference on Computer Vision Workshops*, 2019, pp. 832–839. doi:10.1109/ICCVW.2019.00111.
- [39] X. Huang, X. Cheng, Q. Geng, B. Cao, D. Zhou, P. Wang, Y. Lin, R. Yang, The apolloscape dataset for autonomous driving, in: *Proceedings of the IEEE Conference on Computer Vision and Pattern Recognition Workshops*, 2018, pp. 954–960. doi:10.1109/CVPRW.2018.00141.
- [40] F. Yu, H. Chen, X. Wang, W. Xian, Y. Chen, F. Liu, V. Madhavan, T. Darrell, Bdd100k: A diverse driving dataset for heterogeneous multitask learning, in: *Proceedings of the IEEE/CVF Conference on Computer Vision and Pattern Recognition*, 2020, pp. 2636–2645. doi:10.1109/CVPR42600.2020.00271.
- [41] H. Xu, S. Wang, X. Cai, W. Zhang, X. Liang, Z. Li, Curvelane-nas: Unifying lane-sensitive architecture search and adaptive point blending, in: *European Conference on Computer Vision*, Springer, 2020, pp. 689–704. doi:10.1007/978-3-030-58555-6\_41.
- [42] YouTube, <https://www.youtube.com/> (Accessed: 2024).
- [43] R. Zhang, J. Peng, W. Gou, Y. Ma, J. Chen, H. Hu, W. Li, G. Yin, Z. Li, A robust and real-time lane detection method in low-light scenarios to advanced driver assistance systems, *Expert Systems with Applications* 256 (2024) 124923. doi:10.1016/j.eswa.2024.124923.
- [44] K. Harald, *Theorie der horizontalen sichtweite: Kontrast und sichtweite*, Keim and Nemnich, Munich 12 (1924) 33–53. doi:10.1007/978-3-663-04661-5\_2.
- [45] X. Chen, Y. Wang, X. Chen, W. Zeng, S2r-depthnet: Learning a generalizable depth-specific structural representation, in: *Proceedings of the IEEE/CVF Conference on Computer Vision and Pattern Recognition*, 2021, pp. 3034–3043. doi:10.1109/CVPR46437.2021.00305.
- [46] K. He, J. Sun, X. Tang, Single image haze removal using dark channel prior, *IEEE Transactions on Pattern Analysis and Machine Intelligence* 33 (12) (2011) 2341–2353. doi:10.1109/TPAMI.2010.168.
- [47] J. Wang, K. Sun, T. Cheng, B. Jiang, C. Deng, Y. Zhao, D. Liu, Y. Mu, M. Tan, X. Wang, W. Liu, B. Xiao, Deep high-resolution representation learning for visual recognition, *IEEE Transactions on Pattern Analysis and Machine Intelligence* 43 (10) (2021) 3349–3364. doi:10.1109/TPAMI.2020.2983686.
- [48] Z. Liu, Y. Lin, Y. Cao, H. Hu, Y. Wei, Z. Zhang, S. Lin, B. Guo, Swin transformer: Hierarchical vision transformer using shifted windows, in: *Proceedings of the IEEE/CVF International Conference on Computer Vision*, 2021, pp. 10012–10022. doi:10.1109/ICCV48922.2021.00986.
- [49] A. Dosovitskiy, L. Beyer, A. Kolesnikov, D. Weissenborn, X. Zhai, T. Unterthiner, M. Dehghani, M. Minderer, G. Heigold, S. Gelly, et al., An image is worth 16x16 words: Transformers for image recognition at scale, in: *International Conference on Learning Representations*, 2021, pp. 1–17.
- [50] Z. Tian, B. Zhang, H. Chen, C. Shen, Instance and panoptic segmentation using conditional convolutions, *IEEE*

Transactions on Pattern Analysis and Machine Intelligence 45 (1) (2023) 669–680. doi:10.1109/TPAMI.2022.3145407.

- [51] S. Wang, J. Liu, X. Cao, Z. Song, K. Sun, Polar r-cnn: End-to-end lane detection with fewer anchors, IEEE Transactions on Intelligent Transportation Systems (2025) 1–13doi:10.1109/TITS.2025.3564979.